JOURNAL OF GUIDANCE, CONTROL, AND DYNAMICS
Vol. 28, No. 4, July–August 2005

Calibration and Attitude Determination with Redundant Inertial Measurement Units

Mark E. Pittelkau*
Johns Hopkins University, Applied Physics Laboratory, Laurel, Maryland 20723-6099

A calibration filter is developed for redundant inertial measurement units, which are inertial measurement units that have more than three sense axes. It is shown that for a Kalman filter based on an attitude measurement model and an attitude kinematics model in the "model replacement mode," a linear combination of the calibration parameters is not observable and therefore cannot be estimated. This observability problem is not related to dynamic observability, which requires calibration maneuvers. A null-space measurement equation, together with the attitude measurement and kinematics models, provides complete observability so that all calibration parameters can be estimated. Estimator performance without and with the null-space measurement update is demonstrated via simulation results.

Introduction

ALIGNMENT and calibration of attitude and rate sensors is vital to achieving high performance in a spacecraft attitude determination system. A calibration error model may comprise orthogonal misalignment of attitude sensors, misalignment of the sense axes of an inertial measurement unit (IMU), bias, and symmetric and asymmetric scale factor errors in each IMU sense axis. An attitude determination (Kalman) filter based on an attitude kinematics model augmented with the calibration error model may be used to estimate the calibration parameters. Such calibration filters have been designed for three-axis IMUs.[1–3] In this paper we consider the calibration of an attitude determination system comprising a redundant IMU (RIMU) and attitude sensors.

A RIMU is an IMU that has more than three sense axes; we are not concerned with functional redundancy of the electronics. All sense axes are active in the present context and we assume that the RIMU senses angular rate in all three spatial dimensions. The Northrop–Grumman (formerly Litton) space inertial reference unit (SIRU), which comprises four hemispherical resonator gyros, is an example of a RIMU. The axis orientations of the first-generation SIRU and the second-generation SIRU are shown in Figs. 1a and 1b. A pair of IMUs operating simultaneously, each containing at least three sense axes, also falls under the definition of a RIMU even though the IMUs are in separate housings. This is illustrated in Figs. 1c and 1d. The skew arrangement of two IMUs in Fig. 1c is optimally redundant, whereas the parallel arrangement in Fig. 1d, which is commonly found on spacecraft, is not optimal. One optimal arrangement of n gyros has one gyro along a cone axis and $n-1$ gyros equally spaced on the cone with half-angle $\cos^{-1}\sqrt{[(n-3)/(3n-3)]}$ (Refs. 4 and 5). Another arrangement has any number of gyros equally spaced on a cone with half angle $\cos^{-1}\sqrt{(1/3)}$. These geometries include symmetric arrangements of 4, 3, 4, 6, and 10 gyros in a tetrahedron, hexahedron (cube), octahedron, dodecahedron, and icosahedron. These regular polyhedra are the Platonic solids, of which there are only five. Various optimum RIMU geometries are discussed in Refs. 4 and 5, and examples can be found in Refs. 6–11. Geometry for RIMUs comprising two degree-of-freedom gyros, such as the dry-tuned rotor units from Kearfott, is discussed in Ref. 12.

A RIMU is used in systems that demand high availability, accuracy, and redundancy. Many spacecraft carry a pair of three-axis IMUs that are not normally operated simultaneously and are calibrated separately. Their interlock (relative alignment) can be estimated by treating them as a single redundant six-axis IMU. Calibration of both IMUs simultaneously can result in more precise and more consistent calibration with fewer calibration maneuvers, thereby minimizing interruption of operation of the spacecraft and reducing the ground support cost of calibration.

Attitude dynamics may be modeled by the quaternion kinematic equation

$$\frac{\mathrm{d}\boldsymbol{q}}{\mathrm{d}t} = \frac{1}{2}\bar{\boldsymbol{\omega}} \otimes \boldsymbol{q}, \qquad \bar{\boldsymbol{\omega}} = \begin{bmatrix} \boldsymbol{\omega}^b \\ 0 \end{bmatrix} \tag{1}$$

where $\boldsymbol{\omega}^b$ is the inertial angular rate in body coordinates and $\boldsymbol{q}$ is the attitude quaternion that describes the orientation of the spacecraft body frame with respect to an inertial frame. The attitude measurement is of the form

$$\boldsymbol{y} = \boldsymbol{h}(\boldsymbol{q}) \tag{2}$$

The body angular rates $\boldsymbol{\omega}^b = [\omega_x^b, \omega_y^b, \omega_z^b]^T$ are measured by

$$\boldsymbol{\omega}^m = \boldsymbol{G}\boldsymbol{\omega}^b - \boldsymbol{e} \tag{3}$$

where $\boldsymbol{G}$ is the $n \times 3$ mapping matrix whose rows are the nominal direction vectors of the n sense axes written in body coordinates, $\boldsymbol{\omega}^m = [\boldsymbol{\omega}_1^m, \boldsymbol{\omega}_2^m, \ldots, \boldsymbol{\omega}_n^m]^T$ is a vector of measured angular rates, and $\boldsymbol{e}$ is a vector of errors due to noise, bias, scale factor error, and misalignment. The body angular rate $\boldsymbol{\omega}^b$ is obtained through the pseudoinverse $\boldsymbol{G}^\dagger = (\boldsymbol{G}^T\boldsymbol{G})^{-1}\boldsymbol{G}^T$ such that

$$\boldsymbol{\omega}^b = \boldsymbol{G}^\dagger(\boldsymbol{\omega}^m + \boldsymbol{e}) \tag{4}$$

(The inverse of $\boldsymbol{G}^T\boldsymbol{G}$ exists because we have already assumed that $\boldsymbol{G}$ is full column rank; i.e., the redundant IMU senses rates in all three spatial dimensions. Having all sense axes in a plane would violate this assumption.) We now substitute the angular rate from Eq. (4) into the attitude kinematics model, Eq. (1), whereupon the measurement noise in the gyro becomes process noise in the attitude kinematics model. This substitution is known as "model replacement"[13] because otherwise we would have to use Euler's equation of motion to model the dynamics of the spacecraft.

It should be evident that because $\boldsymbol{G}^\dagger$ is a $3 \times n$ matrix, there is a linear combination $\boldsymbol{e}_N$ of the errors $\boldsymbol{e}$ for which $\boldsymbol{G}^\dagger\boldsymbol{e}_N = \boldsymbol{0}$ when

Received 13 December 2003; presented as AAS Paper 04-116 at the AAS/AIAA Space Flight Mechanics Meeting, Maui, HI, 8–12 February 2004; revision received 29 June 2004; accepted for publication 2 July 2004. Copyright © 2004 by the American Institute of Aeronautics and Astronautics, Inc. The U.S. Government has a royalty-free license to exercise all rights under the copyright claimed herein for Governmental purposes. All other rights are reserved by the copyright owner. Copies of this paper may be made for personal or internal use, on condition that the copier pay the $10.00 per-copy fee to the Copyright Clearance Center, Inc., 222 Rosewood Drive, Danvers, MA 01923; include the code 0731-5090/05 $10.00 in correspondence with the CCC.

*Senior Professional Staff, Guidance and Control Group, Space Department; Mark.Pittelkau@jhuapl.edu, mpittelkau@ieee.org. Associate Fellow AIAA.

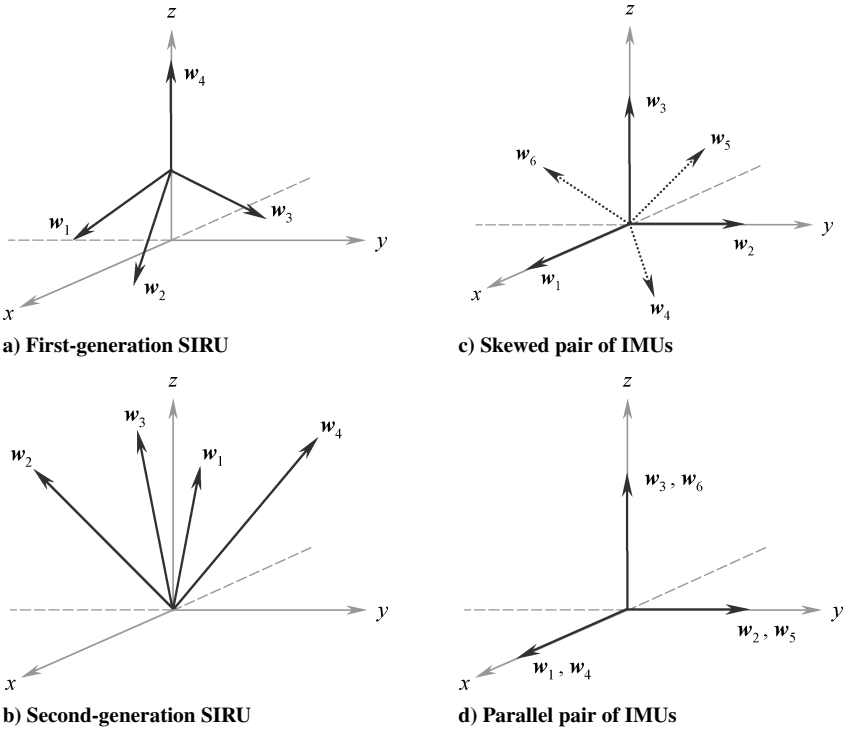

Fig. 1 Some redundant IMU configurations.

$n > 3$, in fact any $\boldsymbol{e}_N$ in the right null space of $\boldsymbol{G}^\dagger$ (the left null space of $\boldsymbol{G}$). Therefore one should expect that a linear combination of gyro biases, scale factor errors, and misalignments does not affect the attitude quaternion $\boldsymbol{q}$ in Eq. (1) and is not observable in measurements of attitude in Eq. (2). It is shown in Ref. 9 that $n-3$ linear combinations of n biases and $3n-9$ linear combinations of $3n$ scale factors and misalignments are observable in the null space. (Only symmetric scale factors were considered in Ref. 9.) Conversely, only three linear combinations of n biases and nine linear combinations of $3n$ scale factors and misalignments are observable in attitude, that is, through the left range space of $\boldsymbol{G}$, which is the orthogonal complement of the left null space of $\boldsymbol{G}$. Thus, using only Eqs. (1), (2), and (4) in the calibration (Kalman) filter leaves the null space unobservable in the model. This is not related to dynamic observability, which requires attitude maneuvers to make the calibration parameters observable. It can be shown that if scale factors are not estimated and no sense axes are parallel, then all misalignments are dynamically observable for $n \leq 4$ with only the measurement models in Eqs. (2) and (4). Simulation results and other analyses show that asymmetric scale factors are fully observable through the left range space of $\boldsymbol{G}$ and unobservable through its left null space. Observability is discussed further in Refs. 9 and 10 and demonstrated in the Results section of this paper.

A calibration filter incorporating a fully observable model is developed in this paper and demonstrated via simulation results. Full observability is achieved with a null-space rate measurement model. The relationship between the null-space rate measurements and the parity vector used in fault detection and isolation (FDI) in inertial navigation systems is discussed in Appendix A.

A suboptimal least-squares calibration method for RIMUs is found in Ref. 14. A calibration filter for RIMUs was developed in Ref. 15, but results were shown for only three gyro axes; for RIMUs it was suggested that the calibration be repeated for every combination of three (noncoplanar) axes. A calibration filter was developed in Refs. 16–19 for the SIRU on the Aqua (EOS PM-1) spacecraft and simulation results were presented. The filter requires knowledge of all torques on the spacecraft (disturbance torque and wheel or other control torque), wheel momentum, and spacecraft inertia, which are generally not known accurately. The true gyro bias vector that was simulated has no component in the left null space of the body-to-gyro mapping matrix $\boldsymbol{G}$.

Before continuing, it is important to ponder an obvious question: Why should we care about an unobservable linear combination of parameters that does not affect attitude? For systems requiring high availability of IRU measurements, it may be intolerable to wait for reconvergence of parameters when one or more gyro axes are lost. Likewise, two IMUs are not coaligned and calibrated if some misalignments and scale-factor errors or combination thereof are not estimated due to lack of observability; often one of the two IMUs is turned off during normal operation on a spacecraft. Furthermore, if the covariances do not converge to a small value due to unobservability, we cannot know the accuracy of the observable part of the estimated parameters. The covariance matrix can be ill conditioned if a linear combination of covariances converges to a small value while another linear combination remains large. Estimates of unobservable parameters and their covariance can drift, thereby potentially causing numerical problems in the Kalman filter. In systems that require high availability and reliability, we need to estimate all parameters so that gyro performance can be monitored. A bad gyro may exhibit increased drift or scale factor error, for example. For these reasons it is important to obtain a fully observable model of the system.

Calibration Model

Calibration models were derived in Refs. 1 and 2 and in Refs. 15–19. We rederive them here in a more general way and with new notation.

The angular rate ω_i^g at the ith gyro axis is given by the projection of the body angular rate $\boldsymbol{\omega}^b$ onto the ith gyro axes $\bar{\boldsymbol{w}}_i$:

$$\omega_i^g = \bar{\boldsymbol{w}}_i \cdot \boldsymbol{\omega}^b = \bar{\boldsymbol{w}}_i^T \boldsymbol{\omega}^b \tag{5}$$

We stack n of these into a vector to form the $n \times 1$ sensed angular rate vector $\boldsymbol{\omega}^g$:

$$\boldsymbol{\omega}^g = \begin{bmatrix} \omega_1^g \\ \omega_2^g \\ \vdots \\ \omega_n^g \end{bmatrix} = \begin{bmatrix} \bar{\boldsymbol{w}}_1^T \\ \bar{\boldsymbol{w}}_2^T \\ \vdots \\ \bar{\boldsymbol{w}}_n^T \end{bmatrix} \boldsymbol{\omega}^b = \bar{\boldsymbol{W}}^T \boldsymbol{\omega}^b = \bar{\boldsymbol{G}} \boldsymbol{\omega}^b \tag{6}$$

where $\bar{\boldsymbol{W}} = [\bar{\boldsymbol{w}}_1, \bar{\boldsymbol{w}}_2, \ldots, \bar{\boldsymbol{w}}_n]$ and $\bar{\boldsymbol{G}} = \bar{\boldsymbol{W}}^T$.

The vectors $\bar{\boldsymbol{w}}_i$ represent the true directions of the gyro sense axes. We know only the nominal vectors $\boldsymbol{w}_i$, which can be related to the true vectors by a small-angle transformation

$$\bar{\boldsymbol{w}}_i = (\boldsymbol{I} + [\boldsymbol{\delta}_i\times])\boldsymbol{w}_i = \boldsymbol{w}_i - [\boldsymbol{w}_i\times]\boldsymbol{\delta}_i \tag{7}$$

where $\boldsymbol{\delta}_i$ is a small-angle rotation vector. Note that any component of $\boldsymbol{\delta}_i$ in the direction of $\boldsymbol{w}_i$ has no effect, so $\boldsymbol{\delta}_i$ has the minimal parameterization

$$\boldsymbol{\delta}_i = \delta_{ui}\boldsymbol{u}_i - \delta_{vi}\boldsymbol{v}_i \tag{8}$$

where $\boldsymbol{u}_i$, $\boldsymbol{v}_i$, and $\boldsymbol{w}_i$ are a mutually orthogonal triad and where δ_{ui} and δ_{vi} are small-angle rotations about the axes $\boldsymbol{u}_i$ and $\boldsymbol{v}_i$. From Eq. (8) we have the misalignment model

$$\bar{\boldsymbol{w}}_i = \boldsymbol{w}_i - \delta_{ui}\boldsymbol{v}_i - \delta_{vi}\boldsymbol{u}_i \tag{9}$$

The vectors $\bar{\boldsymbol{w}}_i$ may be normalized by dividing by $(1+\delta_{ui}^2+\delta_{vi}^2)^{1/2}$. This is not necessary because scale factors can absorb this normalization. One only needs to be consistent in applying the model to avoid introducing errors into the calibrated gyro measurements.

We shall later need the matrices

$$\boldsymbol{U} = [\boldsymbol{u}_1 \quad \boldsymbol{u}_2 \quad \cdots \quad \boldsymbol{u}_n] \tag{10a}$$

$$\boldsymbol{V} = [\boldsymbol{v}_1 \quad \boldsymbol{v}_2 \quad \cdots \quad \boldsymbol{v}_n] \tag{10b}$$

$$\boldsymbol{W} = [\boldsymbol{w}_1 \quad \boldsymbol{w}_2 \quad \cdots \quad \boldsymbol{w}_n] \tag{10c}$$

The nonunique orthonormal basis vectors $\boldsymbol{u}_i$ and $\boldsymbol{v}_i$ can be computed easily using the QR decomposition with pivoting (Ref. 20, pp. 211–236) of the matrices $\boldsymbol{I}-\boldsymbol{w}_i\boldsymbol{w}_i^T$ or of the 3×3 matrices $[\boldsymbol{w}_i \ \ \boldsymbol{0} \ \ \boldsymbol{0}]$, though care should be taken to ensure, for the sake of consistency, that the triad $[\boldsymbol{u}_i \ \ \boldsymbol{v}_i \ \ \boldsymbol{w}_i]$ is right-handed. The vectors $\boldsymbol{u}_i$ and $\boldsymbol{v}_i$ can be any right-handed orthonormal pair in the plane perpendicular to $\boldsymbol{w}_i$, but once chosen they must be fixed. Analytic expressions for $\boldsymbol{u}_i$ and $\boldsymbol{v}_i$ can be derived for specific IMU geometries. Another method of computing $\boldsymbol{u}_i$ and $\boldsymbol{v}_i$ is described in Refs. 16–19.

For n gyro axes, we have from Eqs. (6) and (9) the misalignment model

$$\begin{bmatrix}\omega_1^g\\ \omega_2^g\\ \vdots\\ \omega_n^g\end{bmatrix} = \begin{bmatrix}\boldsymbol{w}_1^T\\ \boldsymbol{w}_2^T\\ \vdots\\ \boldsymbol{w}_n^T\end{bmatrix}\boldsymbol{\omega}^b - \begin{bmatrix}\boldsymbol{\omega}^b\cdot\boldsymbol{v}_1 & \boldsymbol{0} & \boldsymbol{0} & \boldsymbol{0}\\ \boldsymbol{0} & \boldsymbol{\omega}^b\cdot\boldsymbol{v}_2 & \cdots & \boldsymbol{0}\\ \vdots & \vdots & \ddots & \vdots\\ \boldsymbol{0} & \boldsymbol{0} & \cdots & \boldsymbol{\omega}^b\cdot\boldsymbol{v}_n\end{bmatrix}\begin{bmatrix}\delta_{u1}\\ \delta_{u2}\\ \vdots\\ \delta_{un}\end{bmatrix}$$

$$- \begin{bmatrix}\boldsymbol{\omega}^b\cdot\boldsymbol{u}_1 & \boldsymbol{0} & \cdots & \boldsymbol{0}\\ \boldsymbol{0} & \boldsymbol{\omega}^b\cdot\boldsymbol{u}_2 & \cdots & \boldsymbol{0}\\ \vdots & \vdots & \ddots & \vdots\\ \boldsymbol{0} & \boldsymbol{0} & \cdots & \boldsymbol{\omega}^b\cdot\boldsymbol{u}_n\end{bmatrix}\begin{bmatrix}\delta_{v1}\\ \delta_{v2}\\ \vdots\\ \delta_{vn}\end{bmatrix} \tag{11}$$

or more compactly,

$$\boldsymbol{\omega}^g = \boldsymbol{W}^T\boldsymbol{\omega}^b - \boldsymbol{C}_v(\boldsymbol{\omega}^b)\boldsymbol{\delta}_u - \boldsymbol{C}_u(\boldsymbol{\omega}^b)\boldsymbol{\delta}_v \tag{12}$$

where $\boldsymbol{\delta}_u = [\delta_{u1}, \delta_{u2}, \ldots, \delta_{un}]^T$ and $\boldsymbol{\delta}_v = [\delta_{v1}, \delta_{v2}, \ldots, \delta_{vn}]^T$.

The measured angular rate from the ith gyro is given by

$$\omega_i^m = \left(1 - \lambda_i - \mu_i \operatorname{sign}\left(\omega_i^g\right)\right)\omega_i^g - b_i - \eta_i \tag{13}$$

where b_i is the bias, λ_i is the symmetric scale factor error, μ_i is the asymmetric scale factor error, and η_i is white noise. We stack the ω_i^m into a vector to get the RIMU measurement model

$$\boldsymbol{\omega}^m = (\boldsymbol{I} - \boldsymbol{\Lambda} - \mathbf{M})\boldsymbol{\omega}^g - \boldsymbol{b} - \boldsymbol{\eta} \tag{14}$$

where $\boldsymbol{b} = [b_1, b_2, \ldots, b_n]^T$, $\boldsymbol{\eta} = [\eta_1, \eta_2, \ldots, \eta_n]^T$, $\boldsymbol{\Lambda} = \operatorname{diag}(\lambda_1, \lambda_2, \ldots, \lambda_n)$, and $\mathbf{M} = \operatorname{diag}(\mu_1 s_1, \mu_2 s_2, \ldots, \mu_n s_n)$ with $s_i = \operatorname{sign}(\omega_i^g)$. At this point we can define the $5n\times 1$ calibration parameter vector $\boldsymbol{p}$ as

$$\boldsymbol{p} = \begin{bmatrix}\boldsymbol{b}\\ \boldsymbol{\lambda}\\ \boldsymbol{\mu}\\ \boldsymbol{\delta}_u\\ \boldsymbol{\delta}_v\end{bmatrix} \tag{15}$$

where $\boldsymbol{\lambda} = [\lambda_1, \lambda_2, \ldots, \lambda_n]^T$ and $\boldsymbol{\mu} = [\mu_1, \mu_2, \ldots, \mu_n]^T$.

Now define $\boldsymbol{\Delta}_u = \operatorname{diag}(\delta_{u1}, \delta_{u2}, \ldots, \delta_{un})$ and $\boldsymbol{\Delta}_v = \operatorname{diag}(\delta_{v1}, \delta_{v2}, \ldots, \delta_{vn})$. From Eq. (9), we have

$$\bar{\boldsymbol{W}} = \boldsymbol{W} - \boldsymbol{U}\boldsymbol{\Delta}_v - \boldsymbol{V}\boldsymbol{\Delta}_u \tag{16}$$

Equations (11) and (12) can now be written

$$\boldsymbol{\omega}^g = (\boldsymbol{W} - \boldsymbol{U}\boldsymbol{\Delta}_v - \boldsymbol{V}\boldsymbol{\Delta}_u)^T\boldsymbol{\omega}^b = \bar{\boldsymbol{G}}\boldsymbol{\omega}^b \tag{17}$$

From Eqs. (14) and (17) we get

$$\bar{\boldsymbol{G}}\boldsymbol{\omega}^b = (\boldsymbol{I} - \boldsymbol{\Lambda} - \mathbf{M})^{-1}(\boldsymbol{\omega}^m + \boldsymbol{b} + \boldsymbol{\eta}) \tag{18}$$

In the model replacement mode of the attitude determination filter, $\boldsymbol{\omega}^m$ is assumed to be known and $\boldsymbol{\omega}^b$ is a function of $\boldsymbol{\omega}^m$ and $\boldsymbol{p}$. Thus we also need the partial derivative of $\boldsymbol{\omega}^b$ with respect to $\boldsymbol{p}$. From Eq. (18) we have

$$\frac{\partial}{\partial\boldsymbol{p}^T}\bar{\boldsymbol{G}}\boldsymbol{\omega}^b = \frac{\partial}{\partial\boldsymbol{p}^T}(\boldsymbol{I} - \boldsymbol{\Lambda} - \mathbf{M})^{-1}(\boldsymbol{\omega}^m + \boldsymbol{b} + \boldsymbol{\eta}) \tag{19}$$

from which we obtain, with the aid of Eq. (12),

$$\bar{\boldsymbol{G}}\frac{\partial\boldsymbol{\omega}^b}{\partial\boldsymbol{p}^T} - [\boldsymbol{0} \quad \boldsymbol{0} \quad \boldsymbol{0} \quad \boldsymbol{C}_v \quad \boldsymbol{C}_u]$$

$$= (\boldsymbol{I} - \boldsymbol{\Lambda} - \mathbf{M})^{-1}\left[\boldsymbol{I} \quad \operatorname{diag}\left(\omega_i^g\right) \quad \operatorname{diag}\left(\left|\omega_i^g\right|\right) \quad \boldsymbol{0} \quad \boldsymbol{0}\right] \tag{20}$$

Although it is not strictly necessary, it is convenient in the development in the next section to combine the scale factor matrix with $\bar{\boldsymbol{G}}$, so we have

$$\boldsymbol{G}\frac{\partial\boldsymbol{\omega}^b}{\partial\boldsymbol{p}^T} = \boldsymbol{C} \tag{21}$$

where

$$\boldsymbol{G} = (\boldsymbol{I} - \boldsymbol{\Lambda} - \mathbf{M})\bar{\boldsymbol{G}} = (\boldsymbol{I} - \boldsymbol{\Lambda} - \mathbf{M})(\boldsymbol{W} - \boldsymbol{U}\boldsymbol{\Delta}_v - \boldsymbol{V}\boldsymbol{\Delta}_u)^T \tag{22}$$

and where

$$\boldsymbol{C} = \left[\boldsymbol{I} \ \operatorname{diag}\left(\omega_i^g\right) \ \operatorname{diag}\left(\left|\omega_i^g\right|\right) \ (\boldsymbol{I} - \boldsymbol{\Lambda} - \mathbf{M})\boldsymbol{C}_v(\boldsymbol{\omega}^b) \ (\boldsymbol{I} - \boldsymbol{\Lambda} - \mathbf{M})\boldsymbol{C}_u(\boldsymbol{\omega}^b)\right] \tag{23}$$

From Eqs. (18) and (22) we have

$$\boldsymbol{G}\boldsymbol{\omega}^b = \boldsymbol{\omega}^m + \boldsymbol{b} + \boldsymbol{\eta} \tag{24}$$

and from Eqs. (21) and (22) we obtain the sensitivity matrix

$$\frac{\partial\boldsymbol{\omega}^b}{\partial\boldsymbol{p}^T} = \boldsymbol{G}^\dagger\boldsymbol{C} \tag{25}$$

where both $\boldsymbol{G}$ and $\boldsymbol{C}$ depend on the parameter vector $\boldsymbol{p}$ and $\boldsymbol{C}$ depends also on the angular rates $\boldsymbol{\omega}^g$ and $\boldsymbol{\omega}^b$, which are also functions of $\boldsymbol{p}$. (In Ref. 21, $\boldsymbol{C}$ is an approximation and $\boldsymbol{G}$ is constant.)

Calibration Filter

A fully observable formulation of the measurement model is introduced in the next section and then an extended Kalman filter formulation is derived. The model could also be implemented in a least-squares algorithm. An optimal least-squares algorithm for RIMUs is an extension of the algorithm in Ref. 22, but we will not pursue its development here. The Kalman filter developed in the following sections is preferred for reasons of simplicity, for ease of modeling of process noise, and for autonomous real-time calibration.

Fully Observable Formulation

An orthogonal basis $\boldsymbol{N}$ for the left null space of $\boldsymbol{G}$ has the properties

$$\boldsymbol{N}^T\boldsymbol{G} = \boldsymbol{0} \tag{26a}$$

$$\boldsymbol{N}^T\boldsymbol{N} = \boldsymbol{I} \tag{26b}$$

We augment Eq. (24) with the null-space basis $\boldsymbol{N}$ to get

$$[\boldsymbol{G} \quad \boldsymbol{N}]\begin{bmatrix}\boldsymbol{\omega}^b \\ \boldsymbol{0}\end{bmatrix} = \boldsymbol{\omega}^m + \boldsymbol{b} + \boldsymbol{\eta} \tag{27}$$

This augmentation does not change the equation, but we now have a square full-rank matrix $[\boldsymbol{G} \ \boldsymbol{N}]$. Because this matrix is invertible, we can solve Eq. (27) to obtain

$$\begin{bmatrix}\boldsymbol{\omega}^b \\ \boldsymbol{0}\end{bmatrix} = \begin{bmatrix}\boldsymbol{G}^\dagger \\ \boldsymbol{N}^T\end{bmatrix}(\boldsymbol{\omega}^m + \boldsymbol{b} + \boldsymbol{\eta}) \tag{28}$$

The first row of Eq. (28) is the range-space equation

$$\boldsymbol{\omega}^b = \boldsymbol{G}^\dagger(\boldsymbol{\omega}^m + \boldsymbol{b} + \boldsymbol{\eta}) \tag{29a}$$

and the second row of Eq. (28) is the null-space equation

$$\boldsymbol{0} = z = \boldsymbol{N}^T(\boldsymbol{\omega}^m + \boldsymbol{b} + \boldsymbol{\eta}) \tag{29b}$$

A procedure for computing the null-space basis $\boldsymbol{N}$ and the pseudoinverse of $\boldsymbol{G}$ is given in Ref. 20, pp. 211–236, although analytical expressions can be obtained for specific sensor geometries.[6–11]

We have to show that the process noise $\boldsymbol{G}^\dagger\boldsymbol{\eta}$ in Eq. (29a) and the measurement error $\boldsymbol{N}^T\boldsymbol{\eta}$ in Eq. (29b) are uncorrelated, so that the null-space measurement can be used directly in a Kalman filter without resort to modified gain and covariance equations.[23] The error term in Eq. (28) is

$$\varepsilon = \begin{bmatrix}\boldsymbol{G}^\dagger \\ \boldsymbol{N}^T\end{bmatrix}\boldsymbol{\eta} \tag{30}$$

The covariance matrix of the noise vector $\boldsymbol{\eta}$ is

$$\mathcal{E}\{\boldsymbol{\eta}\boldsymbol{\eta}^T\} = \boldsymbol{\Sigma} \tag{31}$$

where $\mathcal{E}\{\cdot\}$ is the expectation operator. The covariance of ε is easily calculated to be

$$\mathcal{E}\{\varepsilon\varepsilon^T\} = \begin{bmatrix}(\boldsymbol{G}^T\boldsymbol{G})^{-1}\boldsymbol{G}^T\boldsymbol{\Sigma}\boldsymbol{G}(\boldsymbol{G}^T\boldsymbol{G})^{-1} & (\boldsymbol{G}^T\boldsymbol{G})^{-1}\boldsymbol{G}^T\boldsymbol{\Sigma}\boldsymbol{N} \\ \boldsymbol{N}^T\boldsymbol{\Sigma}\boldsymbol{G}(\boldsymbol{G}^T\boldsymbol{G})^{-1} & \boldsymbol{N}^T\boldsymbol{\Sigma}\boldsymbol{N}\end{bmatrix} \tag{32}$$

The measurement error and the process noise are uncorrelated if and only if $(\boldsymbol{G}^T\boldsymbol{G})^{-1}\boldsymbol{G}^T\boldsymbol{\Sigma}\boldsymbol{N} = \boldsymbol{0}$. This holds for the general form $\boldsymbol{\Sigma} = \boldsymbol{G}(\boldsymbol{G}^T\boldsymbol{G})^{-1/2}\boldsymbol{\Sigma}_1[\boldsymbol{G}(\boldsymbol{G}^T\boldsymbol{G})^{-1/2}]^T + \boldsymbol{N}\boldsymbol{\Sigma}_2\boldsymbol{N}^T$, where $\boldsymbol{\Sigma}_1$ is a 3×3 covariance matrix and $\boldsymbol{\Sigma}_2$ is an $(n-3)\times(n-3)$ covariance matrix. For isotropic error, $\boldsymbol{\Sigma}_1 = \sigma^2\boldsymbol{I}_3$ and $\boldsymbol{\Sigma}_2 = \sigma^2\boldsymbol{I}_{n-3}$, so that $\boldsymbol{\Sigma} = \sigma^2\boldsymbol{I}_n$, and the covariance of ε is

$$\mathcal{E}\{\varepsilon\varepsilon^T\} = \sigma^2\begin{bmatrix}(\boldsymbol{G}^T\boldsymbol{G})^{-1} & \boldsymbol{0} \\ \boldsymbol{0} & \boldsymbol{I}\end{bmatrix} \tag{33}$$

General, Fully Observable Formulation

We will now remove the restriction that the gyro errors be isotropic. Nonisotropic errors may exist if two IMUs of different types and performance are operated simultaneously or if some axes in a redundant IMU fail gracefully and exhibit greater noise output than other axes.

Factor the RIMU noise covariance matrix $\boldsymbol{\Sigma}$ such that $\boldsymbol{X}\boldsymbol{X}^T = \boldsymbol{\Sigma}$ and define

$$\boldsymbol{G}_\Sigma = \boldsymbol{X}^{-1}\boldsymbol{G} \tag{34}$$

The weighted left null-space matrix $\boldsymbol{N}_\Sigma$ is such that $\boldsymbol{N}_\Sigma^T\boldsymbol{G}_\Sigma = \boldsymbol{0}$ and $\boldsymbol{N}_\Sigma^T\boldsymbol{N}_\Sigma = \boldsymbol{I}$. The matrices $\boldsymbol{N}_\Sigma$ and $\boldsymbol{G}_\Sigma^\dagger$ are computed from $\boldsymbol{G}_\Sigma$ in the same way that $\boldsymbol{N}$ and $\boldsymbol{G}^\dagger$ are computed from $\boldsymbol{G}$. Relationships between $\boldsymbol{G}_\Sigma^\dagger$ and $\boldsymbol{G}^\dagger$ and between $\boldsymbol{N}_\Sigma$ and $\boldsymbol{N}$ are shown in Appendix B.

We now premultiply Eq. (24) by $\boldsymbol{X}^{-1}$ and then augment it using $\boldsymbol{N}_\Sigma$. Solving the system of equations yields the weighted range-space equation

$$\boldsymbol{\omega}^b = \boldsymbol{G}_\Sigma^\dagger\boldsymbol{X}^{-1}(\boldsymbol{\omega}^m + \boldsymbol{b} + \boldsymbol{\eta}) \tag{35a}$$

and the weighted null-space equation

$$\boldsymbol{0} = z = \boldsymbol{N}_\Sigma^T\boldsymbol{X}^{-1}(\boldsymbol{\omega}^m + \boldsymbol{b} + \boldsymbol{\eta}) \tag{35b}$$

The error term is

$$\varepsilon = \begin{bmatrix}\boldsymbol{G}_\Sigma^\dagger \\ \boldsymbol{N}_\Sigma^T\end{bmatrix}\boldsymbol{X}^{-1}\boldsymbol{\eta} \tag{36}$$

from which we easily calculate the covariance of error to be

$$\mathcal{E}\{\varepsilon\varepsilon^T\} = \begin{bmatrix}(\boldsymbol{G}^T\boldsymbol{\Sigma}^{-1}\boldsymbol{G})^{-1} & \boldsymbol{0} \\ \boldsymbol{0} & \boldsymbol{I}\end{bmatrix} \tag{37}$$

Because the off-diagonal blocks are zero, the process noise $\boldsymbol{G}_\Sigma^\dagger\boldsymbol{X}^{-1}\boldsymbol{\eta}$ in the weighted range-space equation (35a) and the measurement error $\boldsymbol{N}_\Sigma^T\boldsymbol{X}^{-1}\boldsymbol{\eta}$ in the weighted null-space measurement equation (35b) are uncorrelated. Thus the null-space measurement equation (35b) may be used directly in a Kalman filter. Furthermore, it is significant that null-space measurement error has a diagonal covariance, namely the identity matrix $\boldsymbol{I}$, because the Agee–Turner measurement update algorithm[24] can be applied directly as part of a square-root implementation of the filter.

The weighted range-space sensitivity matrix that corresponds to Eq. (35a) is obtained by premultiplying Eq. (21) by $\boldsymbol{X}^{-1}$ to obtain

$$\frac{\partial\boldsymbol{\omega}^b}{\partial\boldsymbol{p}^T} = \boldsymbol{G}_\Sigma^\dagger\boldsymbol{X}^{-1}\boldsymbol{C} \tag{38a}$$

The weighted null-space sensitivity matrix that corresponds to Eq. (35b) is

$$\frac{\partial\boldsymbol{z}}{\partial\boldsymbol{p}^T} = \boldsymbol{N}_\Sigma^T\boldsymbol{X}^{-1}\boldsymbol{C} \tag{38b}$$

Attitude Measurement Model

Although the attitude kinematics was written in terms of the quaternion and its time derivative in Eq. (1), for many practical reasons we do not advocate using the quaternion as a filter state.[25–28] Instead, a small-angle rotation vector $\tilde{\boldsymbol{\phi}}$ (perturbation state) models the true attitude $\boldsymbol{q}$ relative to a nearby reference attitude.[13,29,30] The reference attitude is the a priori attitude estimate $\hat{\boldsymbol{q}}$ in an extended Kalman filter. Thus we have

$$\boldsymbol{q} = \boldsymbol{q}(\tilde{\phi}) \otimes \hat{\boldsymbol{q}} \tag{39}$$

In general, an attitude sensor may be parameterized with a small-angle rotation vector $\boldsymbol{\delta}_j = \hat{\boldsymbol{\delta}}_j + \tilde{\boldsymbol{\delta}}_j$ to model misalignment, where the subscript j denotes the jth attitude sensor, $\hat{\boldsymbol{\delta}}_j$ is the a priori estimate, and $\tilde{\boldsymbol{\delta}}_j$ is the perturbation state. The attitude measurement model has the general form

$$\boldsymbol{y}_j = \boldsymbol{h}(\tilde{\boldsymbol{\delta}}_j, \hat{\boldsymbol{\delta}}_j, \tilde{\boldsymbol{\phi}}, \hat{\boldsymbol{q}}) + \boldsymbol{\nu}_j \tag{40}$$

where $\boldsymbol{\nu}_j$ is white measurement noise with covariance $\mathcal{E}\{\boldsymbol{\nu}_j\boldsymbol{\nu}_j^T\} = \boldsymbol{\Sigma}_{\nu j}$. It is shown in Refs. 1 and 2 how to derive the measurement sensitivity matrix for quaternion, vector, and focal plane measurement models. The derivation of the measurement sensitivity matrix for quaternion measurements may be somewhat obscure in Ref. 1 and is made clearer in Ref. 29. The sensitivity of $\boldsymbol{y}_j$ to attitude is

$$H_\phi^{(j)} = \frac{\partial\boldsymbol{y}_j}{\partial\tilde{\boldsymbol{\phi}}^T} = \frac{\partial}{\partial\tilde{\boldsymbol{\phi}}^T}\boldsymbol{h}(\tilde{\boldsymbol{\delta}}_j, \hat{\boldsymbol{\delta}}_j, \tilde{\boldsymbol{\phi}}, \hat{\boldsymbol{q}}) \tag{41}$$

and the sensitivity of $\boldsymbol{y}_j$ to misalignment is

$$H_{\delta_j}^{(j)} = \frac{\partial \boldsymbol{y}_j}{\partial \boldsymbol{\delta}_j^T} = \frac{\partial}{\partial \tilde{\boldsymbol{\delta}}_j^T} \boldsymbol{h}(\tilde{\boldsymbol{\delta}}_j, \hat{\boldsymbol{\delta}}_j, \tilde{\boldsymbol{\phi}}, \hat{\boldsymbol{q}}) \tag{42}$$

These sensitivity matrices are evaluated at $\tilde{\boldsymbol{\phi}} = \boldsymbol{0}$ and $\tilde{\boldsymbol{\delta}}_j = \boldsymbol{0}$. For m attitude sensors, we can write the measurements, misalignments, and measurement noise as tall vectors:

$$\boldsymbol{y} = \begin{bmatrix} \boldsymbol{y}_1 \\ \boldsymbol{y}_2 \\ \vdots \\ \boldsymbol{y}_m \end{bmatrix}, \qquad \boldsymbol{\delta} = \begin{bmatrix} \boldsymbol{\delta}_1 \\ \boldsymbol{\delta}_2 \\ \vdots \\ \boldsymbol{\delta}_m \end{bmatrix}, \qquad \boldsymbol{\nu} = \begin{bmatrix} \boldsymbol{\nu}_1 \\ \boldsymbol{\nu}_2 \\ \vdots \\ \boldsymbol{\nu}_m \end{bmatrix} \tag{43}$$

and the corresponding measurement sensitivity matrices are

$$\boldsymbol{H}_\phi = \begin{bmatrix} H_\phi^{(1)} \\ H_\phi^{(2)} \\ \vdots \\ H_\phi^{(m)} \end{bmatrix}, \qquad \boldsymbol{H}_\delta = \begin{bmatrix} H_{\delta 1}^{(1)} & \boldsymbol{0} & \cdots & \boldsymbol{0} \\ \boldsymbol{0} & H_{\delta 2}^{(2)} & \cdots & \boldsymbol{0} \\ \vdots & \vdots & \ddots & \vdots \\ \boldsymbol{0} & \boldsymbol{0} & \cdots & H_{\delta m}^{(m)} \end{bmatrix} \tag{44}$$

The covariance of the measurement error vector $\boldsymbol{\nu}$ is

$$\boldsymbol{\Sigma}_\nu = \mathcal{E}\{\boldsymbol{\nu}\boldsymbol{\nu}^T\} = \begin{bmatrix} \boldsymbol{\Sigma}_{\nu 1} & \boldsymbol{0} & \cdots & \boldsymbol{0} \\ \boldsymbol{0} & \boldsymbol{\Sigma}_{\nu 2} & \cdots & \boldsymbol{0} \\ \vdots & \vdots & \ddots & \vdots \\ \boldsymbol{0} & \boldsymbol{0} & \cdots & \boldsymbol{\Sigma}_{\nu m} \end{bmatrix} \tag{45}$$

From these definitions, we can write the linearized measurement model with the first-order approximation

$$\tilde{\boldsymbol{y}} = \boldsymbol{y} - \hat{\boldsymbol{y}} \simeq \boldsymbol{H}_\phi \tilde{\boldsymbol{\phi}} + \boldsymbol{H}_\delta \tilde{\boldsymbol{\delta}} + \boldsymbol{\nu} \tag{46}$$

where $\hat{\boldsymbol{y}} = \boldsymbol{h}(\hat{\bar{\boldsymbol{\delta}}}, \hat{\boldsymbol{\delta}}, \hat{\bar{\boldsymbol{\phi}}}, \hat{\boldsymbol{q}})$ and where $\hat{\bar{\boldsymbol{\delta}}}$, $\hat{\bar{\boldsymbol{\phi}}}$, $\hat{\boldsymbol{\delta}}$, and $\hat{\boldsymbol{q}}$ are a priori estimates with $\hat{\bar{\boldsymbol{\delta}}} = \boldsymbol{0}$ and $\hat{\bar{\boldsymbol{\phi}}} = \boldsymbol{0}$. Naturally we will use the nonlinear measurement equation (40) to compute the residual in the extended Kalman filter. For quaternion "measurements," the residual should be computed as the principal rotation vector from the predicted measurement $\hat{\boldsymbol{y}}$ to the actual measurement.[29]

Putting It All Together

The estimated angular rate is given by the expectation of Eq. (35a) conditioned on past measurements, which is approximately [because Eq. (35a) is nonlinear]

$$\hat{\boldsymbol{\omega}}^b = \boldsymbol{\omega}^b|_{p=\hat{p}} = \hat{\boldsymbol{G}}_\Sigma^\dagger \boldsymbol{X}^{-1}(\boldsymbol{\omega}^m + \hat{\boldsymbol{b}}) \tag{47}$$

where $\hat{\boldsymbol{G}}_\Sigma$ is given by Eq. (34) with $\boldsymbol{G}$ defined in Eq. (22) evaluated at the a priori estimate $\hat{\boldsymbol{p}} = \hat{\boldsymbol{p}}_{k|k-1}$. Following Ref. 13 or Ref. 29, the linearized attitude dynamics equation is

$$\frac{\mathrm{d}\tilde{\boldsymbol{\phi}}}{\mathrm{d}t} = -\hat{\boldsymbol{\omega}}^b \times \tilde{\boldsymbol{\phi}} + \tilde{\boldsymbol{\omega}}^b \tag{48}$$

where $\tilde{\boldsymbol{\phi}}$ is a small-angle rotation vector (attitude perturbation) and where $\tilde{\boldsymbol{\omega}}^b = \boldsymbol{\omega}^b - \hat{\boldsymbol{\omega}}^b$. Expanding $\boldsymbol{\omega}^b$ in a Taylor series about $\hat{\boldsymbol{p}}$ yields, to first order in $\tilde{\boldsymbol{p}} = \boldsymbol{p} - \hat{\boldsymbol{p}}$,

$$\begin{aligned} \tilde{\boldsymbol{\omega}}^b &= \left(\boldsymbol{\omega}^b|_{p=\hat{p}} + \left.\frac{\partial \boldsymbol{\omega}^b}{\partial \boldsymbol{p}^T}\right|_{p=\hat{p}} \tilde{\boldsymbol{p}} \right) - \hat{\boldsymbol{\omega}}^b \\ &= \left.\frac{\partial \boldsymbol{\omega}^b}{\partial \boldsymbol{p}^T}\right|_{p=\hat{p}} \tilde{\boldsymbol{p}} + \hat{\boldsymbol{G}}_\Sigma^\dagger \boldsymbol{X}^{-1} \boldsymbol{\eta} \end{aligned} \tag{49}$$

Substituting this into Eq. (48), with the partial derivative given by Eq. (38a), yields the attitude dynamics model

$$\frac{\mathrm{d}\tilde{\boldsymbol{\phi}}}{\mathrm{d}t} = -\hat{\boldsymbol{\omega}}^b \times \tilde{\boldsymbol{\phi}} + \hat{\boldsymbol{G}}_\Sigma^\dagger \boldsymbol{X}^{-1} \hat{\boldsymbol{C}} \tilde{\boldsymbol{p}} + \hat{\boldsymbol{G}}_\Sigma^\dagger \boldsymbol{X}^{-1} \boldsymbol{\eta} \tag{50}$$

Equation (50) is accurate to first order in the perturbation states $\tilde{\boldsymbol{\phi}}$ and $\tilde{\boldsymbol{p}}$. Second-order linearization errors and nonlinear stochastic effects can produce biased estimates in an extended Kalman filter, but results have not revealed any significant bias.

The state perturbation equations are

$$\boldsymbol{\phi} = \tilde{\boldsymbol{\phi}} \circ \hat{\boldsymbol{\phi}} \tag{51a}$$

$$\boldsymbol{p} = \hat{\boldsymbol{p}} + \tilde{\boldsymbol{p}} \tag{51b}$$

$$\boldsymbol{\delta} = \hat{\boldsymbol{\delta}} + \tilde{\boldsymbol{\delta}} \tag{51c}$$

The composition of rotation vectors in Eq. (51a) can be effectively computed by the quaternion composition (see Ref. 29, Appendix)

$$\boldsymbol{q}(\boldsymbol{\phi}) = \boldsymbol{q}(\tilde{\boldsymbol{\phi}} \circ \hat{\boldsymbol{\phi}}) = \boldsymbol{q}(\tilde{\boldsymbol{\phi}}) \otimes \boldsymbol{q}(\hat{\boldsymbol{\phi}}) \tag{52}$$

where $\boldsymbol{q}(\cdot)$ is the quaternion computed from its argument.

The gyro calibration parameters and attitude sensor misalignments are assumed to be constant, but we introduce a small amount of white process noise to model slow variations in the parameters and to ensure numerical stability of the covariance update. The gyro bias components of the parameter vector are driven by a larger process noise and may be modeled with a Markov model rather than a random walk model. The random walk model is usually adequate and is preferred for simplicity. The dynamics of the parameters are thus modeled by

$$\frac{\mathrm{d}\boldsymbol{p}}{\mathrm{d}t} = \boldsymbol{\eta}_p \tag{53a}$$

$$\frac{\mathrm{d}\boldsymbol{\delta}}{\mathrm{d}t} = \boldsymbol{\eta}_\delta \tag{53b}$$

where $\boldsymbol{\eta}_p$ and $\boldsymbol{\eta}_\delta$ are white noise processes with covariance $\mathcal{E}\{\boldsymbol{\eta}_p \boldsymbol{\eta}_p^T\} = \boldsymbol{\Sigma}_p$ and $\mathcal{E}\{\boldsymbol{\eta}_\delta \boldsymbol{\eta}_\delta^T\} = \boldsymbol{\Sigma}_\delta$. These covariance matrices are usually diagonal.

We can now write a single differential equation for the dynamics of the state, gyro parameters, and sensor alignments from Eqs. (50), (53a), and (53b):

$$\begin{aligned} \frac{\mathrm{d}}{\mathrm{d}t} \begin{bmatrix} \tilde{\boldsymbol{\phi}} \\ \tilde{\boldsymbol{p}} \\ \tilde{\boldsymbol{\delta}} \end{bmatrix} &= \begin{bmatrix} -[\hat{\boldsymbol{\omega}}^b \times] & \hat{\boldsymbol{G}}_\Sigma^\dagger \boldsymbol{X}^{-1} \hat{\boldsymbol{C}} & \boldsymbol{0} \\ \boldsymbol{0} & \boldsymbol{0} & \boldsymbol{0} \\ \boldsymbol{0} & \boldsymbol{0} & \boldsymbol{0} \end{bmatrix} \begin{bmatrix} \tilde{\boldsymbol{\phi}} \\ \tilde{\boldsymbol{p}} \\ \tilde{\boldsymbol{\delta}} \end{bmatrix} \\ &\quad + \begin{bmatrix} \hat{\boldsymbol{G}}_\Sigma^\dagger \boldsymbol{X}^{-1} & \boldsymbol{0} & \boldsymbol{0} \\ \boldsymbol{0} & \boldsymbol{I} & \boldsymbol{0} \\ \boldsymbol{0} & \boldsymbol{0} & \boldsymbol{I} \end{bmatrix} \begin{bmatrix} \boldsymbol{\eta} \\ \boldsymbol{\eta}_p \\ \boldsymbol{\eta}_\delta \end{bmatrix} \end{aligned} \tag{54}$$

The linearized attitude measurement model and the null-space rate measurement model can be combined into one equation:

$$\begin{bmatrix} \tilde{\boldsymbol{y}} \\ \tilde{\boldsymbol{z}} \end{bmatrix} = \begin{bmatrix} \boldsymbol{H}_\phi & \boldsymbol{0} & \boldsymbol{H}_\delta \\ \boldsymbol{0} & \hat{\boldsymbol{N}}_\Sigma^T \boldsymbol{X}^{-1} \hat{\boldsymbol{C}} & \boldsymbol{0} \end{bmatrix} \begin{bmatrix} \tilde{\boldsymbol{\phi}} \\ \tilde{\boldsymbol{p}} \\ \tilde{\boldsymbol{\delta}} \end{bmatrix} + \begin{bmatrix} \boldsymbol{\nu} \\ \hat{\boldsymbol{N}}_\Sigma^T \boldsymbol{X}^{-1} \boldsymbol{\eta} \end{bmatrix} \tag{55}$$

From Eq. (35b), the null-space measurement prediction is

$$\hat{\boldsymbol{z}} = \hat{\boldsymbol{N}}_\Sigma^T \boldsymbol{X}^{-1}(\hat{\boldsymbol{\omega}}^m + \hat{\boldsymbol{b}}) \tag{56}$$

Noting that because the null-space rate measurement is $\boldsymbol{z} = \boldsymbol{0}$, the weighted null-space measurement residual is simply $\tilde{\boldsymbol{z}} = \boldsymbol{z} - \hat{\boldsymbol{z}} = -\hat{\boldsymbol{z}}$.

For the nonredundant system of $n = 3$ gyro axes, we have $\boldsymbol{G}_\Sigma^\dagger \boldsymbol{X}^{-1} = \boldsymbol{G}^{-1}$ and the null-space measurement equation vanishes (its dimension is zero), so the model reduces to essentially the one in the calibration filter in Ref. 1. (In the present model the asymmetric scale factor is included and the symmetric scale factor is modeled separately from the gyro misalignments.)

Model-Order Reduction

The IMU and attitude sensor alignment parameters overparameterize the alignments so that there are three unobservable degrees of freedom, one in each of the three body axes.[1,2] The three unobservable degrees of freedom are removed by choosing one of the attitude sensors or the IMU as the reference sensor, which is not parameterized with a misalignment vector and which defines the body reference frame.[2] It was shown in Ref. 2 how to reduce the order of the IMU alignment model when the IMU is the reference sensor. This is not so obvious for a RIMU. A means to reduce the order of the RIMU alignment model is the subject of Ref. 31.

It is well known that a linear combination of parameters in the null space of $\boldsymbol{G}$ can be estimated with angular rates only,[9,10,32–34] and so one should be able to partition the model such that a linear combination of parameters observable through the left range space of $\boldsymbol{G}$ is estimated in the Kalman filter and an orthogonal linear combination of parameters observable through the left null space of $\boldsymbol{G}$ is estimated in a separate filter using only rate measurements. Such a partitioning is beyond the scope of this paper.

Attitude Determination with Redundant Gyros

A real-time attitude determination filter usually contains only attitude and gyro bias states. With redundant gyros, the attitude determination filter can be obtained by removing all calibration parameters except the biases b_i from the calibration model. This leaves $\boldsymbol{C}=\boldsymbol{I}$ and $\boldsymbol{p}=\boldsymbol{b}$. Equations (35a) and (35b) and their sensitivities in Eqs. (38a) and (38b) are unchanged except that $\boldsymbol{G}$ and $\boldsymbol{N}$ are constant.

In the case of a nonredundant system of $n=3$ gyro axes, $\boldsymbol{G}_\Sigma^\dagger \boldsymbol{X}^{-1}=\boldsymbol{G}^{-1}$ and the null-space measurement equation vanishes, so the model reduces to the one in the usual six-state attitude determination filter[13,29] that comprises three attitude perturbation states and three gyro bias states. Note that in both Refs. 13 and 29 it was assumed that $\boldsymbol{G}=\boldsymbol{I}$. The formulation here is completely general.

Implementation

The calibration filter was implemented using the modified weighted Gram–Schmidt (MWGS) and Agee–Turner algorithms for covariance factor propagation and update.[24] The factorized process noise matrix and covariance factor propagation were implemented in a manner similar to that described in Refs. 1 and 2. The filter is essentially an extension of those reported in Refs. 1 and 2 with the addition of the null-space measurement update.

Because most gyros produce incremental angle (integrated rate) measurements instead of rate measurements, the measurement model, Eq. (6), has to be rewritten in terms of incremental angle measurements

$$\boldsymbol{\theta}_k^g=\int_{t_{k-1}}^{t_k}\boldsymbol{\omega}^g(t)\,\mathrm{d}t$$

where t_{k-1} and t_k are the sample times of the attitude measurement. We then have the range-space and null-space estimates

$$\hat{\boldsymbol{\theta}}_k^b=\hat{\boldsymbol{G}}_\Sigma^\dagger\boldsymbol{X}^{-1}\left(\boldsymbol{\theta}_k^m+T_k\hat{\boldsymbol{b}}_{k|k-1}\right) \tag{57}$$

$$\hat{\boldsymbol{z}}_k=\hat{\boldsymbol{N}}_\Sigma^T\boldsymbol{X}^{-1}\left(\boldsymbol{\theta}_k^m+T_k\hat{\boldsymbol{b}}_{k|k-1}\right) \tag{58}$$

where $T_k=t_k-t_{k-1}$ and where $\boldsymbol{\theta}_k^b$ is the integrated body angular-rate vector over the interval t_{k-1} to t_k. In practice the vector $\boldsymbol{\theta}_k^m$ comprises, for each gyro, the sum of the measured angular increments from time t_{k-1} to time t_k. The discrete-time measurement error

$$\boldsymbol{\eta}_k=\int_{t_{k-1}}^{t_k}\boldsymbol{\eta}(t)\,\mathrm{d}t$$

has covariance $T_k\boldsymbol{\Sigma}$. Because the RIMU measurements are angular increments rather than rates, the sensitivity matrix in Eq. (23) becomes

$$\boldsymbol{C}_k=\left[T_k\boldsymbol{I}\ \operatorname{diag}\left(\theta_i^g\right)\ \operatorname{diag}\left(\left|\theta_i^g\right|\right)\ (\boldsymbol{I}-\boldsymbol{\Lambda}-\boldsymbol{M})\boldsymbol{C}_v\left(\boldsymbol{\theta}_k^b\right)\ (\boldsymbol{I}-\boldsymbol{\Lambda}-\boldsymbol{M})\boldsymbol{C}_u\left(\boldsymbol{\theta}_k^b\right)\right] \tag{59}$$

Note that $\int|\omega_i^g|\,\mathrm{d}t\geq|\int\omega_i^g\,\mathrm{d}t|=|\theta_i^g|$. Thus an error occurs when ω_i^g changes sign during the integration interval. This error is small if the integration interval is small and inconsequential because the zero crossings are infrequent for calibration maneuvers.

It is a matter of convenience that the null-space measurement update be performed at the time of the attitude update. It could be performed at other times or less frequently than the attitude updates, although there does not seem to be any significant computational advantage in doing so. The angular increment can be over an interval shorter than the time between attitude measurements, as long as the discrete-time null-space measurement covariance is scaled accordingly.

Calibration Filter Results

The system considered comprises two star trackers and a RIMU with four gyro axes. For generality, rotational misalignment is modeled at each sensor. We choose star tracker 1 to be the reference sensor, and so the misalignment of star tracker 1 is set to zero and is not estimated. This prevents three degrees of freedom of attitude from being unobservable.[2] Sensor parameters and filter initialization parameters are given in the next subsection and the calibration maneuver is defined. Estimation results are then given, first without the null-space measurement update to illustrate the lack of observability discussed in the Introduction. Estimation results are then given to demonstrate that all parameters are estimated correctly when updated with the null-space measurement.

Parameters

The IMU geometry is the SIRU configuration in Refs. 16–19, which is Fig. 1a rotated 90 deg about the z axis. The nominal $\boldsymbol{U}$, $\boldsymbol{V}$, and $\boldsymbol{W}$ matrices for this configuration are

$$\boldsymbol{U}=\begin{bmatrix}-\sqrt{1/3} & -\sqrt{5/6} & -\sqrt{5/6} & 1\\ 0 & -\sqrt{1/10} & \sqrt{1/10} & 0\\ -\sqrt{2/3} & \sqrt{1/15} & \sqrt{1/15} & 0\end{bmatrix}$$

$$\boldsymbol{V}=\begin{bmatrix}0 & 0 & 0 & 0\\ 1 & \sqrt{2/5} & \sqrt{2/5} & 1\\ 0 & \sqrt{3/5} & -\sqrt{3/5} & 0\end{bmatrix}$$

$$\boldsymbol{W}=\begin{bmatrix}\sqrt{2/3} & -\sqrt{1/6} & -\sqrt{1/6} & 0\\ 0 & \sqrt{1/2} & -\sqrt{1/2} & 0\\ -\sqrt{1/3} & -\sqrt{1/3} & -\sqrt{1/3} & 1\end{bmatrix} \tag{60}$$

The matrices $\boldsymbol{U}$ and $\boldsymbol{V}$ are given because they are not uniquely determined from $\boldsymbol{W}$. A basis for the left null space of $\boldsymbol{G}_o=\boldsymbol{W}^T$ is

$$\boldsymbol{N}_o=\begin{bmatrix}\sqrt{1/6} & \sqrt{1/6} & \sqrt{1/6} & \sqrt{1/2}\end{bmatrix}^T \tag{61}$$

The true gyro axis directions are the columns of $\boldsymbol{W}$ rotated by the δ_u and δ_v in Table 1 according to Eq. (9). The initial gyro bias, true scale factors, and true misalignments shown in Table 1 were chosen randomly from a uniform distribution on $[-L, L]$, where L is shown in Table 1. The true gyro bias varies according to a rate random walk process, which is driven by a white noise of variance $\sigma_{\mathrm{rrw}}^2=(2/\tau_s)\sigma_s^2$, where $\sigma_s=0.05$ deg/h (arcsec/s) is the bias stability and $\tau_s=3600$ s is the stability interval. The angle-random-walk process is driven by a white noise of standard deviation $\sigma_{\mathrm{arw}}=0.005\ \mathrm{deg/h}^{1/2}$ and the angle white noise at the output of the gyros has a standard deviation of 0.2 arcsec. The gyro sampling rate is 100 Hz. Note that these are not the SIRU noise specifications; they were instead chosen to be the same noise parameters used in Refs. 1 and 2.

The star trackers are mounted orthogonally with nominal mounting quaternions

$$\boldsymbol{q}_b^{s1} = \begin{bmatrix} 0.1207549821894208 \\ -0.4456792768263646 \\ 0.2319681614447059 \\ 0.8561419216461720 \end{bmatrix}$$

$$\boldsymbol{q}_b^{s2} = \begin{bmatrix} 0.4456792768263646 \\ -0.1207549821894208 \\ 0.8561419216461720 \\ 0.2319681614447059 \end{bmatrix} \tag{62}$$

The misalignment vector for star tracker 2 is $\boldsymbol{\delta}_{s2} = [2900, -1500, 800]^T$ arcsec. Star tracker 1 defines the body reference frame, so its misalignment is zero ($\boldsymbol{\delta}_{s1} = \mathbf{0}$) and the initial standard deviation of error of the estimate is set to 0.1 arcsec. This value is nonzero to avoid making the initial covariance matrix singular but is small enough that the tracker 1 alignment estimate remains close to zero. It is a matter of convenience to retain an alignment vector in the calibration filter for all attitude sensors even though one is redundant. The accuracy of the star trackers is 6 arcsec cross-boresight and 37 arcsec around its boresight. The star tracker measurements are sampled at 1 Hz. Note that the true calibration parameters in Table 1 and the star tracker misalignments given earlier are large and can occur in practice.

Table 1 True RIMU parameter values

Axis	Bias b, deg/h	ssf λ, ppm	asf μ, ppm	δ_u, arcsec	δ_v, arcsec
1	−1.575	−140.2	−963.0	2101.9	−678.9
2	1.768	3913.0	642.8	3037.0	3135.4
3	0.589	2621.0	−110.6	1715.1	3001.7
4	−1.253	−435.3	230.9	−2330.9	−646.0
L	2.0	5000.0	1000.0	3600.0	3600.0

Table 2 Star tracker alignment estimation performance

Star tracker	Alignment, arcsec		
	x axis	y axis	z axis
1			
Alignment estimate	0.0	0.0	−0.0
Estimation error	−0.0	−0.0	0.0
Standard deviation	0.1	0.1	0.1
2			
Alignment estimate	2899.7	−1500.4	799.5
Estimation error	0.3	0.4	0.5
Standard deviation	0.4	0.5	0.6

The initial attitude estimate is the first quaternion measurement transformed to body coordinates. The initial attitude error covariance is the 3×3 measurement noise covariance plus the covariance of the misalignment of the tracker used for initialization. This total covariance is then transformed to body coordinates. The initial estimates of the parameters are zero and their variance is $(3\sigma)^2 = 3L^2$, where $\sigma^2 = L^2/3$ is the variance of a uniform distribution with L shown in Table 1. For the star tracker misalignment we have $L = 3600$ arcsec.

The standard deviation of the process noise for all parameters, except the gyro bias, has the value 0.001 (ppm/s$^{1/2}$ or arcsec/s$^{1/2}$ as appropriate for each parameter). This value is small enough so that it does not significantly influence the estimates, but is large enough to avoid potential numerical problems by preventing the covariance of any parameter estimate from becoming too small. A square-root formulation of the covariance and gain equations is used, so numerical problems are not likely to occur. Potential problems due to linearization error have not arisen, but if they occur they can be eliminated by local or global relinearization.

Calibration Maneuver

The calibration maneuver, which is aptly described as a "corkscrew" maneuver, exhibits a sinusoidally varying angular rate in each body axis. The angular rate vector is

$$\boldsymbol{\omega}^b(t) = \begin{bmatrix} \omega_{ox} \sin(2\pi\Omega_x t) \\ \omega_{oy} \sin(2\pi\Omega_y t) \\ \omega_{oz} \sin(2\pi\Omega_z t) \end{bmatrix} \tag{63}$$

where $[\omega_{ox}, \omega_{oy}, \omega_{oz}] = [0.3464, 0.2828, 0.2]$ deg/s and $[\Omega_x, \Omega_y, \Omega_z] = [0.00318, 0.00212, 0.00105]$ Hz. The duration of the maneuver is $t_f = 4000$ s. This maneuver ensures that the dynamic observability condition

$$\int_0^{t_f} \boldsymbol{\omega}^b (\boldsymbol{\omega}^b)^T \, \mathrm{d}t > 0$$

is satisfied. A large variety of maneuvers exist that satisfy this condition and are suitable for this example. A discussion of calibration maneuvers is beyond the scope of this paper.

Calibration Filter Results

The calibration filter was run both without and with the null-space measurement update to illustrate the lack of observability discussed in the Introduction. These cases will be referred to as partial and full observability. The same pseudorandom noise sequence was used in each case. Results are shown in Figs. 2 and 3. Estimation errors and the $\pm 1\sigma$ accuracy bounds are shown in the graphs. The $\pm 1\sigma$ bounds are from the square root of the diagonal of the filter's covariance matrix. The final parameter estimates, estimation errors, and standard deviation of error are shown in Tables 2 and 3 for one realization.

Table 3 RIMU calibration performance

Axis	Partial observability					Full observability				
	Bias b, deg/h	ssf λ, ppm	asf μ, ppm	δ_u, arcsec	δ_v, arcsec	Bias b, deg/h	ssf λ, ppm	asf μ, ppm	δ_u, arcsec	δ_v, arcsec
1										
Estimate	−2.026	−1022.4	−954.6	2019.9	−869.7	−1.675	−143.9	−954.7	2101.2	−680.4
Error	0.317	882.2	−8.4	82.0	190.7	−0.034	3.8	−8.2	0.7	1.5
Std dev	0.792	963.8	19.3	167.7	239.9	0.024	9.5	17.1	1.8	2.4
2										
Estimate	1.420	2951.4	635.1	3193.7	3265.0	1.786	3925.5	636.2	3037.5	3133.9
Error	0.395	961.6	7.7	−156.6	−129.6	0.029	−12.6	6.5	−0.5	1.5
Std dev	0.828	1003.0	15.4	257.0	171.7	0.022	10.4	13.9	2.4	1.6
3										
Estimate	0.245	2220.7	−118.8	1448.3	3080.2	0.607	2614.9	−114.1	1711.7	3001.3
Error	0.348	400.3	8.1	266.8	−78.5	−0.013	6.1	3.5	3.4	0.4
Std dev	0.823	1102.7	14.6	244.4	158.9	0.023	9.9	13.4	2.4	1.6
4										
Estimate	−1.794	1851.7	234.2	−2476.7	−720.1	−1.170	−424.5	251.1	−2327.1	−649.7
Error	0.630	−2287.1	−3.4	145.9	74.1	0.006	−10.9	−20.2	−3.8	3.6
Std dev	1.423	2424.5	41.5	302.6	258.7	0.026	13.5	29.2	1.9	1.5

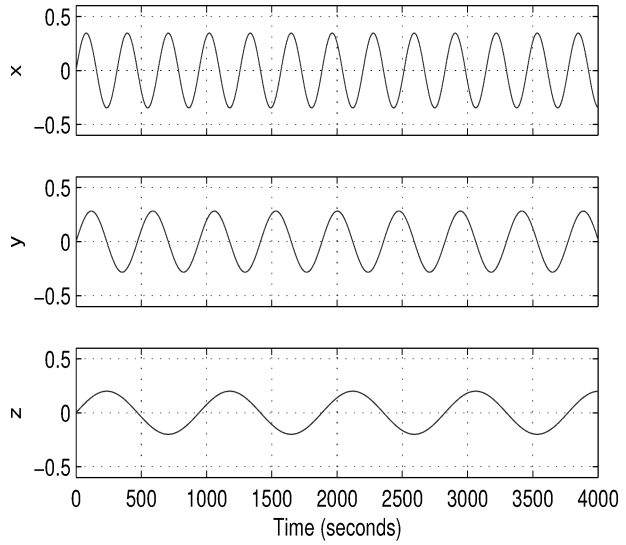

a) Angular rate (deg/s)

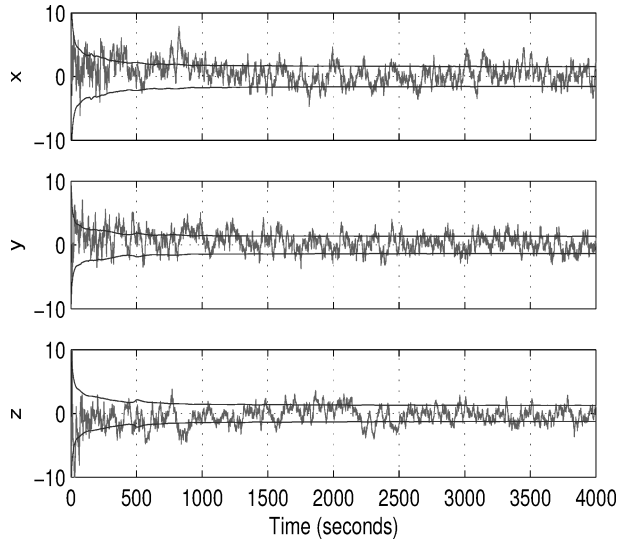

b) Attitude estimate error (arcsec)

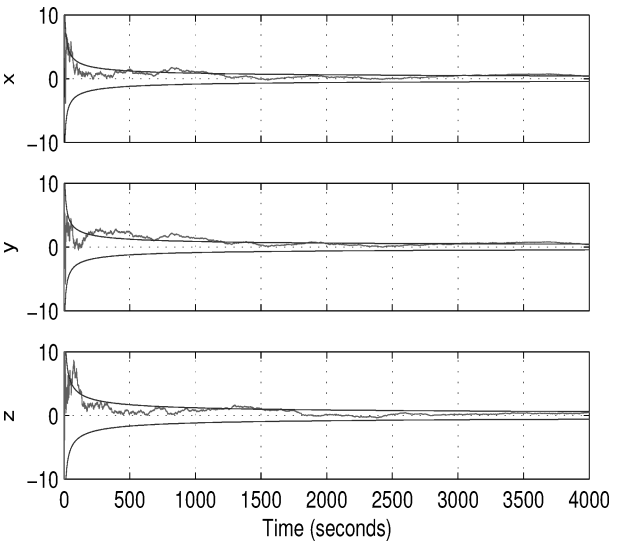

c) Star tracker 2 alignment (arcsec)

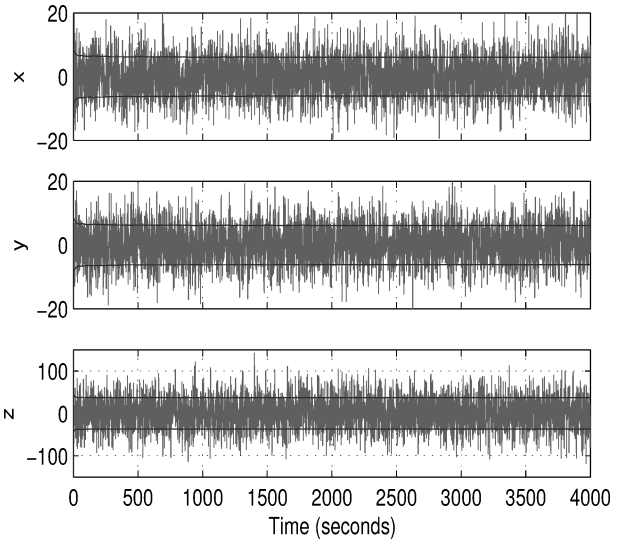

d) Star tracker 2 residuals (arcsec)

Fig. 2 For both partial and full observability: a) calibration maneuver, b) attitude estimation performance, c) star tracker calibration performance, and d) star tracker residuals.

The attitude estimation error, star tracker misalignment estimate error, and star-tracker measurement residuals are identical with partial observability (no null space update) and full observability (with the null space update) as shown in Fig. 2 and Table 2. Those results show good convergence of the estimation error and standard deviation of error in the attitude and star tracker 2 misalignment estimates. The measurement residuals of both star trackers are zero mean with covariance predicted by the filter. (The residuals from star tracker 1 are not shown.) The final estimates of the gyro bias, scale factors, and misalignment estimate errors and their standard deviations are shown in Table 3 for the cases of partial and full observability. The results show that when the null-space measurement update is not performed, the parameter estimate errors, except for the asymmetric scale factor estimate error, do not converge to small values, whereas they do converge to small values when the null-space measurement update is performed. Representative graphs of convergence of the parameter estimation error and standard deviations for the two cases are shown in Figs. 3a and 3b, where the convergence of δ_v is shown. When the filter is not updated with the null-space measurement, the null-space measurement residual shown in Fig. 3c is about 5 arcsec peak and varies with angular rate (it reaches a periodic steady state after 4000 s) and has a corresponding standard deviation as predicted by the filter, even though the attitude estimation error in Fig. 2b does not show any rate dependency. This indicates that the calibration parameters converged in the left range space of $\boldsymbol{G}$ but not completely in the left null space of $\boldsymbol{G}$. The fact that they converged at all in the left null space is possibly due to $\boldsymbol{G}$ changing as the RIMU parameters converged. Figure 3d shows that the null-space measurement residuals are small, zero mean, and uncorrelated when the filter is updated with the null-space measurements.

In the partially observable case, the bias estimate error lies mostly in the null space. From the data in Table 3, we find that the norm of the bias error vector is 0.881 deg/h. The norm of the projection of the bias error vector onto the left null space of $\boldsymbol{G}$ is 0.879 deg/h and the norm of its projection (via $\boldsymbol{I} - \boldsymbol{N}\boldsymbol{N}^T$) onto the left range space of $\boldsymbol{G}$ is 0.0470 deg/h, which is very close to the corresponding result in the fully observable case presented next.

In the fully observable case, the norm of the bias error vector is 0.0469 deg/h. The norm of the projection of the bias error vector onto the left null space of $\boldsymbol{G}$ is 0.0025 deg/h and the norm of its projection onto the left range space of $\boldsymbol{G}$ is 0.0468 deg/h.

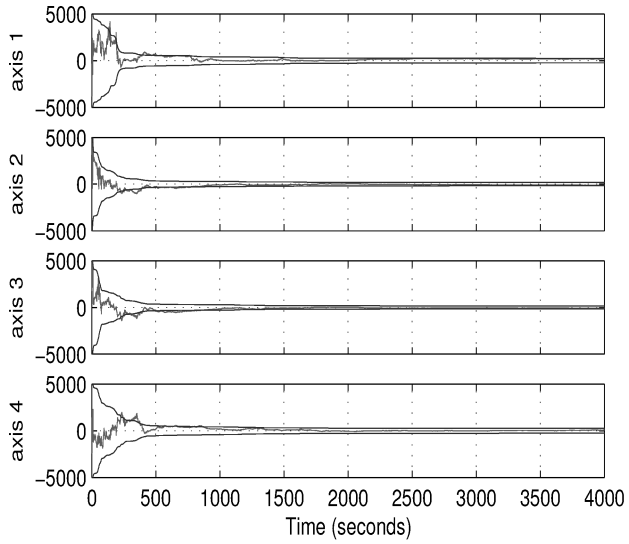

a) Partial observability: δ_v estimate error (arcsec)

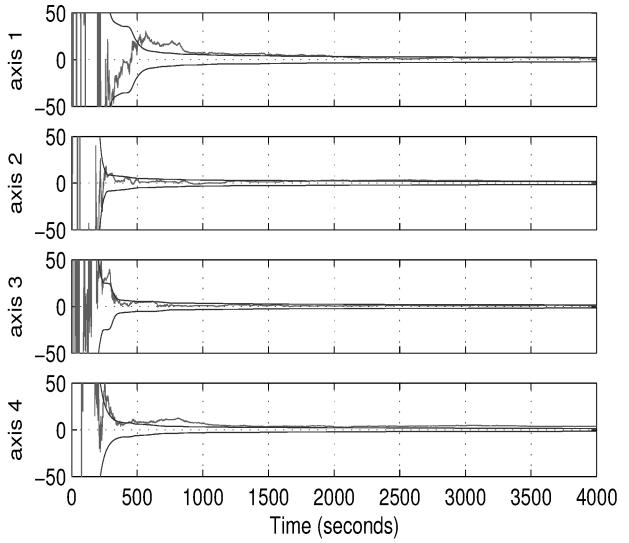

b) Full observability: δ_v estimate error (arcsec)

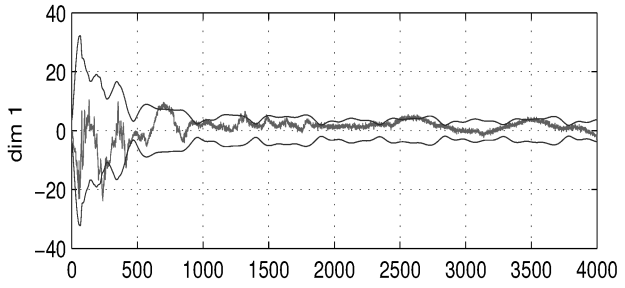

c) Partial observability: null-space residual (arcsec)

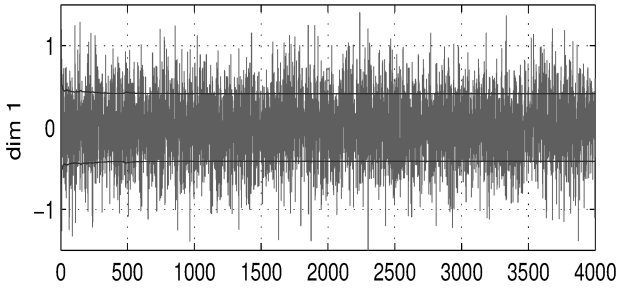

d) Full observability: null-space residual (arcsec)

Fig. 3 RIMU calibration performance with partial and full observability.

Summary

The calibration filter for redundant inertial measurement units (RIMUs) developed in this paper accurately estimates calibration parameters based on a fully observable calibration model operating in the "model replacement" mode (where the gyro measurements replace the dynamics model for angular rate). The calibration parameters of a RIMU are not fully observable in attitude. This is not related to dynamic observability, which requires angular rates that satisfy a dynamic observability criterion. Full observability of the calibration parameters is achieved with a null-space measurement equation, together with the attitude measurement model and attitude dynamics model. The dimension of the null space is $n-3$, where n is the number of sense axes in the RIMU. Calibration filter performance without and with the null-space measurement update is demonstrated with simulation results. These results illustrate that the parameters are not estimated well with attitude measurements alone but can be estimated accurately via null-space measurement updates. The cost of obtaining complete observability is $n-3$ scalar null-space measurement updates each filter cycle (or less frequently). The square-root implementation of the calibration filter is efficient and numerically reliable, and therefore is suitable for on-orbit real-time calibration and attitude determination. A low-order attitude determination filter is obtained by simply eliminating some of the calibration parameters.

Multiplication of the null-space measurement equation by the null-space matrix gives the equation for parity residuals, which are commonly used in navigation systems for fault detection and isolation. The calibration filter for RIMUs provides more reliable fault detection by allowing a smaller fault detection threshold in the presence of wide parameter variations. The estimated parameters can also be trended or compared to limits to detect degradation or failure.

The concept of the null-space measurement equation can be extended to a redundant accelerometer suite in a navigation system where similar null-space observability exists. The null-space accelerometer measurements, together with position or velocity measurements (e.g., global positioning system measurements or Doppler measurements) provide full observability of the calibration parameters.

Appendix A: Relationship Between the Null-Space Measurement and Parity Residuals

Parity residuals are commonly used in aircraft and rocket navigation systems for fault detection and isolation (FDI). The parity equation is given by

$$\boldsymbol{\rho} = \boldsymbol{N}^T\boldsymbol{\omega}^m = \boldsymbol{N}^T(\boldsymbol{G}\boldsymbol{\omega}^b - \boldsymbol{\beta} - \boldsymbol{\eta}) \tag{A1}$$

where $\boldsymbol{\beta} = \boldsymbol{0}$ in the absence of a failed gyro and $\boldsymbol{\beta} \neq \boldsymbol{0}$ in the presence of a failure, and $\boldsymbol{N}^T\boldsymbol{G} = \boldsymbol{0}$. This is essentially Eq. (29b) with $\boldsymbol{p} = \boldsymbol{0}$ and $\boldsymbol{\rho} = -\boldsymbol{N}^T\boldsymbol{\eta}$ in the absence of failure. The body angular rate is computed from the gyro measurements by $\hat{\boldsymbol{\omega}}^b = \boldsymbol{G}^\dagger\boldsymbol{\omega}^m$. Parity residuals are computed as

$$\boldsymbol{\omega}^m - \boldsymbol{G}\hat{\boldsymbol{\omega}}^b = \boldsymbol{\omega}^m - \boldsymbol{G}\boldsymbol{G}^\dagger\boldsymbol{\omega}^m = \boldsymbol{N}\boldsymbol{\rho} \tag{A2}$$

Likelihood ratio tests are generally used to detect when $\boldsymbol{\beta} \neq \boldsymbol{0}$; see Refs. 6–8 and references therein.

Equation (28) can be manipulated to obtain

$$\boldsymbol{\omega}^m = \boldsymbol{W}^T\boldsymbol{\omega}^b - \boldsymbol{\beta} - \boldsymbol{\eta} \tag{A3}$$

where, in the absence of failure but in the presence of miscalibration,

$$\boldsymbol{\beta} = \boldsymbol{b} + [\boldsymbol{W}(\boldsymbol{\Lambda} + \boldsymbol{M}) + \boldsymbol{U}\boldsymbol{\Delta}_v' + \boldsymbol{V}\boldsymbol{\Delta}_u']^T\boldsymbol{\omega}^b \tag{A4}$$

where $\boldsymbol{\Delta}_u' = \boldsymbol{\Delta}_u(\boldsymbol{I} - \boldsymbol{\Lambda} - \mathbf{M})$ and $\boldsymbol{\Delta}_v' = \boldsymbol{\Delta}_v(\boldsymbol{I} - \boldsymbol{\Lambda} - \mathbf{M})$.

As can be seen from the foregoing, the gyros must be calibrated; otherwise the term $\boldsymbol{N}^T\boldsymbol{\beta} \neq \boldsymbol{0}$ will interfere with the failure detection test. Kalman filter and other approaches to parity vector compensation, based only on gyro measurements, have been reported in the literature,[9,10,32–34] where it is recognized that a linear combination of the calibration parameters $\boldsymbol{p}$ is unobservable. FDI with attitude, range, and velocity sensors in navigation systems is discussed in Ref. 8.

Appendix B: Relationship Between $\boldsymbol{G}_{\boldsymbol{\Sigma}}^{\dagger}$ and $\boldsymbol{G}^{\dagger}$ and Between $\boldsymbol{N}_{\boldsymbol{\Sigma}}$ and $\boldsymbol{N}$

In this Appendix we show the relationship between $\boldsymbol{G}_{\Sigma}^{\dagger}$ and $\boldsymbol{G}^{\dagger}$ and between $\boldsymbol{N}_{\Sigma}$ and $\boldsymbol{N}$. We have defined $\boldsymbol{G}_{\Sigma} = \boldsymbol{X}^{-1}\boldsymbol{G}$ and the factorization $\boldsymbol{X}\boldsymbol{X}^T = \boldsymbol{\Sigma}$. We then have $\boldsymbol{\Sigma}^{-1} = (\boldsymbol{X}^{-1})^T\boldsymbol{X}^{-1}$. From these definitions and the definition of the pseudoinverse (see Ref. 20, p. 243) we have

$$\begin{aligned}\boldsymbol{G}_{\Sigma}^{\dagger} &= \left(\boldsymbol{G}_{\Sigma}^T\boldsymbol{G}_{\Sigma}\right)^{-1}\boldsymbol{G}_{\Sigma}^T \\ &= \left(\boldsymbol{G}^T(\boldsymbol{X}^{-1})^T\boldsymbol{X}^{-1}\boldsymbol{G}\right)^{-1}\boldsymbol{G}^T(\boldsymbol{X}^{-1})^T \\ &= (\boldsymbol{G}^T\boldsymbol{\Sigma}^{-1}\boldsymbol{G})^{-1}\boldsymbol{G}^T\boldsymbol{\Sigma}^{-1}\boldsymbol{X} \qquad \text{(B1)}\end{aligned}$$

This shows that $\boldsymbol{G}_{\Sigma}^{\dagger}$ is simply a weighted pseudoinverse of $\boldsymbol{G}$. It is easy to see by direct calculation that $\boldsymbol{G}_{\Sigma}^{\dagger}\boldsymbol{G}_{\Sigma} = \boldsymbol{I}$.

The null-space matrix $\boldsymbol{N}_{\Sigma}$ can be written in terms of $\boldsymbol{N}$ as

$$\boldsymbol{N}_{\Sigma} = \boldsymbol{X}^T\boldsymbol{N}\boldsymbol{S}^{-1} \qquad \text{(B2)}$$

where $\boldsymbol{S}^T\boldsymbol{S} = \boldsymbol{N}^T\boldsymbol{\Sigma}\boldsymbol{N}$ is any convenient factorization of $\boldsymbol{N}^T\boldsymbol{\Sigma}\boldsymbol{N}$. To show that $\boldsymbol{N}_{\Sigma}$ is a basis for the left null space of $\boldsymbol{G}_{\Sigma}$, it suffices to show that $\boldsymbol{N}_{\Sigma}^T\boldsymbol{G}_{\Sigma} = \boldsymbol{0}$ and $\boldsymbol{N}_{\Sigma}^T\boldsymbol{N}_{\Sigma} = \boldsymbol{I}$, which is a straightforward calculation.

The purpose of the foregoing was simply to show some relationships, not to suggest a means of computing $\boldsymbol{G}_{\Sigma}^{\dagger}$ and $\boldsymbol{N}_{\Sigma}$. These are most easily and most accurately computed by the QR decomposition of $\boldsymbol{G}_{\Sigma}$ (see Ref. 20, pp. 211–236).

Acknowledgments

This work was supported by the NASA Goddard Space Flight Center under Contract NAS5-97271. The author graciously acknowledges the diligence and contributions of the second reviewer, in particular for pointing out that the parameter sensitivity matrix in the original draft (and in the conference version of this paper) was actually an approximation to the true derivative.

References

[1]Pittelkau, M. E., "Kalman Filtering for Spacecraft System Alignment Calibration," *Journal of Guidance, Control, and Dynamics*, Vol. 24, No. 6, 2001, pp. 1187–1195.

[2]Pittelkau, M. E., "Everything Is Relative in System Alignment Calibration," *Journal of Spacecraft and Rockets*, Vol. 39, No. 3, 2002, pp. 460–466.

[3]Lam, Q. M., Hunt, T., Sanneman, P., and Underwood, S., "Analysis and Design of a Fifteen State Stellar Inertial Attitude Determination System," *AIAA Guidance, Navigation, and Control Conference and Exhibit* [CD-ROM], AIAA, Reston, VA, 2003 (AIAA Paper 2003-5483).

[4]Sukkarieh, S., Gibbens, P., Grocholsky, B., Willis, K., and Durrant-Whyte, H. F., "A Low-Cost, Redundant Inertial Measurement Unit for Unmanned Air Vehicles," *International Journal of Robotics Research*, Vol. 19, No. 11, 2000, pp. 1089–1103.

[5]Pesja, A. J., "Optimum Orientation and Accuracy of Redundant Sensor Arrays," AIAA Paper 71-59, Jan. 1971.

[6]Daley, K. C., Gai, E., and Harrison, J. V., "Generalized Likelihood Test for FDI in Redundant Sensor Configurations," *Journal of Guidance, Control, and Dynamics*, Vol. 2, No. 1, 1979, pp. 9–17.

[7]Wilcox, J. C., "Competitive Evaluation of Failure Detection Algorithms for Strapdown Redundant Inertial Instruments," *Journal of Spacecraft and Rockets*, Vol. 11, No. 7, 1974, pp. 525–530.

[8]Evans, F. A., and Wilcox, J. C., "Experimental Strapdown Redundant Sensor Inertial Navigation System," *Journal of Spacecraft*, Vol. 7, No. 9, 1970, pp. 1070–1074.

[9]Hall, S. R., "Parity Vector Compensation For FDI," S.M. Thesis, Dept. of Aeronautics and Astronautics, Massachusetts Inst. of Technology, Cambridge, MA, Feb. 1982.

[10]Hall, S. R., Motyka, P., Gai, E., Deyst, J. J., Jr., "In-Flight Parity Vector Compensation For FDI," *IEEE Transactions on Aerospace and Electronic Systems*, Vol. 19, No. 5, 1983, pp. 668–676.

[11]Gilmore, J. P., and McKern, R. A., "A Redundant Strapdown Inertial Reference Unit (SIRU)," *Journal of Spacecraft and Rockets*, Vol. 9, No. 1, 1972, pp. 39–47.

[12]Harrison, J. V., and Gai, E. G., "Evaluating Sensor Orientations for Navigation Performance and Failure Detection," *IEEE Transactions on Aerospace and Electronic Systems*, Vol. 13, No. 6, 1977, pp. 631–643.

[13]Lefferts, E. J., Markley, F. L., snd Shuster, M. D., "Kalman Filtering for Spacecraft Attitude Estimation," *Journal of Guidance, Control, and Dynamics*, Vol. 5, No. 5, 1982, pp. 417–429.

[14]Radomski, M., "On-Orbit Calibration of Redundant Spacecraft Gyros by Optimal Reduction to Three Axes," NASA CP-2001-209986, June 2001, pp. 175–185.

[15]Gray, C. W., Herman, L. K., Kolve, D. I., and Westerlund, G. L., "On-Orbit Attitude Reference Alignment and Calibration," *Advances in the Astronautical Sciences*, Vol. 72, 1990, pp. 275–292.

[16]Harman, R. R., Bar-Itzhack, I. Y., snd Markley, F. L., "Calibration of the Skewed AQUA Satellite Gyros," *Advances in the Astronautical Sciences*, Vol. 109, Pt. 1, 2002, pp. 199–212.

[17]Bar-Itzhack, I. Y., snd Harman, R. R., "In-Space Calibration of a Gyro Quadruplet," NASA CP-2001-209986, June 2001, pp. 229–247.

[18]Bar-Itzhack, I. Y., snd Harman, R. R., "In-Space Calibration of a Gyro Quadruplet," *AIAA Guidance, Navigation, and Control Conference* [CD-ROM], AIAA, Reston, VA, 2001 (AIAA Paper 2001-4152).

[19]Bar-Itzhack, I. Y., and Harman, R. R., "In-Space Calibration of a Skewed Gyro Quadruplet," *Journal of Guidance, Control, and Dynamics*, Vol. 25, No. 5, 2002, pp. 852–859.

[20]Golub, G., and Van Loan, C. F., *Matrix Computations*, 2nd ed., Johns Hopkins Univ. Press, Baltimore, MD, 1989, pp. 211–236, 243.

[21]Pittelkau, M. E., "Attitude Determination and Calibration with Redundant Inertial Measurement Units," *Advances in the Astronautical Sciences*, Vol. 119, Pt. 1, 2004, pp. 229–248.

[22]Davis, S., and Lai, J., "Attitude Sensor Calibration for the Ocean Topography Experiment Satellite," *Space Guidance, Control, and Tracking Conference*, Vol. 1949, Society of Photo-Optical Instrumentation Engineers (International Society for Optical Engineering), Bellingham, WA, 1993, pp. 80–91.

[23]Jazwinski, A. H., *Stochastic Processes and Filtering Theory*, Academic Press, New York, 1970, pp. 209–212, 228.

[24]Bierman, G. J., *Factorization Methods for Discrete Sequential Estimation*, Academic Press, New York, 1977, pp. 76–81, 100, 101, 124–134.

[25]Markley, F. L., "Attitude Estimation or Quaternion Estimation?" *Advances in the Astronautical Sciences*, Vol. 115, 2003, pp. 113–127.

[26]Shuster, M. D., "The Quaternion in the Kalman Filter," *Advances in the Astronautical Sciences*, Vol. 85, 1994, pp. 25–37.

[27]Pittelkau, M. E., "An Analysis of the Quaternion Attitude Determination Filter," *Journal of the Astronautical Sciences*, Vol. 51, No. 1, 2004, pp. 103–120.

[28]Pittelkau, M. E., "Measurement Sensitivity Equations in Attitude Determination," NASA CP-2003-212246, Oct. 2003.

[29]Pittelkau, M. E., "Rotation Vector in Attitude Estimation," *Journal of Guidance, Control, and Dynamics*, Vol. 26, No. 6, 2003, pp. 855–860.

[30]Markley, F. L., "Attitude Error Representations for Kalman Filtering," *Journal of Guidance, Control, and Dynamics*, Vol. 26, No. 2, 2003, pp. 311–317.

[31]Pittelkau, M. E., "RIMU Misalignment Vector Decomposition," AIAA Paper 2004-4856, Aug. 2004.

[32]Dong, Y., and Zhang, H. Y., "Parity Vector Compensation Using Nonlinear Filtering," *Proceedings of IFAC Workshop on Safety, Reliability, and Applications of Emerging Intelligent Control Technologies*, Elsevier, Oxford, 1994, pp. 167–171.

[33]Song, H., and Zhang, H., "An Approach to Sensor Fault Detection Based On Fully Decoupled Parity Equation and Parameter Estimation," *Proceedings of the 4th World Congress on Intelligent Control and Automation*, Vol. 4, Inst. of Electrical and Electronics Engineers, Piscataway, NJ, 2002, pp. 2750–2754.

[34]Ho, J. H., "Sensor Redundancy Management/Fault Detection and Isolation of the Inertial Measurement Unit for a Land-Based Vehicle's Locating System," Ph.D. Dissertation, Dept. of Mechanical Engineering, Pennsylvania State Univ., University Park, PA, Oct. 1999.